



Experimental and modeling study of adsorption–desorption processes with application to a deep-well injection radioactive waste disposal site

V.G. Rumynin^{a,*}, P.K. Konosavsky^a, E. Hoehn^b

^a*Institute of Environmental Geology of Russian Academy of Sciences (RAS), St. Petersburg Division, 14th Line, dom. 29, St. Petersburg, 199178 (Russia)*

^b*Swiss Federal Institute for Environmental Science and Technology, EAWAG, P.O. Box 611, Ueberlandstrasse 133, CH-8600 Duebendorf (Switzerland)*

Received 8 October 2002; received in revised form 5 July 2004; accepted 21 July 2004

Abstract

Radionuclide (Sr-90 and Cs-137) behavior in the subsurface environment was evaluated with respect to natural attenuation, sorption and desorption kinetics, and equilibrium. Batch experiments were conducted with synthesized groundwater or acid (NaNO_3 ; $\text{pH} \approx 3$) solutions under different temperature ($T=20$ and 70 °C) and pressure ($P=P_{\text{atm}}$ and $P=3$ MPa) conditions. Samples of sedimentary rock were selected as the solid phase from a radioactively contaminated site associated with deep-well injection of the radioactive waste. Groundwater and a NaNO_3 waste–brine solution were used as the liquid phase. All experiments revealed hysteresis in radionuclide adsorption. Moreover, some of the experiments indicated that the adsorption process may be irreversible. A simultaneous temperature and pressure increase leads to anomalous behavior of the adsorption kinetics: a period of a rapid concentration drop of the radionuclides in solution, which is caused by their sorption uptake, is changed by a stage of a gradual increase in the corresponding concentrations. To explain the observed phenomena, several hypotheses were examined. Thus, an analytical model describing the mutual interference of adsorption kinetics and dissolution of carbonate minerals was developed resulting in a nonmonotonic behavior of the concentration curves obtained at the adsorption stage. For the description of the batch experiments with

* Corresponding author. Tel.: +7 (812) 321 97 49; fax: +7 (812) 327 49 22.

E-mail address: SlaRum@hydra.nw.ru (V.G. Rumynin).

radionuclides at room temperature and atmospheric pressure, a dual-site adsorption model has been used.

© 2004 Elsevier B.V. All rights reserved.

Keywords: Adsorption hysteresis; Kinetics; Mineral dissolution; Radioactive waste disposal; Sr-90; Cs-137

1. Introduction

The study of the dynamics of processes governing rehabilitation of groundwater quality in periods of natural or forced flow of water through contaminated areas (including sites of radioactive waste disposal) requires the development of models that consider possible hysteresis in adsorption-related processes. Adsorption hysteresis (isotherm nonsingularity) has been a subject of considerable dispute among environmental researchers over the past decades (Pickens et al., 1981; Vandergraaf and Abry, 1982; Jackson and Inch, 1983; Lyon and Patterson, 1984; Vilks and Degueudre, 1991; Streck et al., 1995; Wels et al., 1996; Zakharova et al., 1996; Rumynin et al., 1998; Lisitzin et al., 1999).

Adsorption hysteresis, slow desorption kinetics, and other nonideal phenomena may be attributed to the physical and chemical interactions of dissolved components with soils and sediments. Hysteresis in adsorption is known to be of particular importance for colloid-facilitated transport under natural field conditions (Vilks et al., 1993; Kretzschmar et al., 1999).

To study the existence of hysteresis in radionuclide adsorption, researchers have used batch adsorption/desorption experiment (Vandergraaf and Abry, 1982; Vilks and Degueudre, 1991; Rybalchenko et al., 1994, 1996; Wels et al., 1996; Zakharova et al., 1996; Lisitzin et al., 1999; Rumynin et al., 2002). Data about a low extent of desorption (the first percents to the first tens of percents) were reported in sorption/desorption studies of radionuclides such as Cs-137, Sr-90, Ru-106, Ce-144, Pu-239 on sandy–clayey sediments (Rybalchenko et al., 1994, 1996; Zakharova et al., 1996). The relatively low percentage of desorption of radionuclides is noted in experiments with volcanogenic-sedimentary rocks (Lisitzin et al., 1999). The low degree of extractability of radionuclides was noted for samples of soils selected within areas affected by the Chernobyl accident (Ovsyanikova et al., 2000).

In this context, research in which a numerical comparison of the phase distribution coefficients for equilibrium adsorption, K_d^s and desorption, K_d^d has been analyzed. Vilks and Degueudre (1991), who studied the behavior of Cs-137 and Sr-90 in colloidal systems, have found that K_d^d exceeds K_d^s (for Cs-137) by a factor of 4; a significant hysteresis for Sr-90 was, however, not found. Sorption interaction of ion IO_3^- with clayey minerals (products of weathering of granites which cover fractures) was characterized by the relation of K_d^d to K_d^s , which was within the same range (Tiknor and Cho, 1990).

In the study of radionuclide adsorption (Sr-90, Cs-137, Ce-144 and Pu-239) on surfaces of slabs which were cut from igneous rocks, Vandergraaf and Abry (1982), and Wels et al. (1996), have detected significant differences in K_a^s and K_a^d as well. The same effect was observed in similar experiments on adsorption of Sr-90 onto surfaces of disks

that were cut from the core material of volcanogenic and volcanogenic-sedimentary rocks (Rumynin et al., 1998).

In some investigations dedicated to the study of radionuclide adsorption, a strong kinetic nature of the desorption stage was detected. Sufficiently prolonged periods of a change in the concentration function preceded a new desorption equilibrium. Thus, the relatively slow desorption kinetics of Sr-85 and Sr-90 was identified in field experiments and from analysis of residual radioactivity of cores of contaminated aquifer sediments by Pickens et al. (1981). In contrast, adsorption can be considered from a practical point of view as an equilibrium process (Van de Weerd and Leijnse, 1997). In the opinion of some authors (Rybalchenko et al., 1996; Zakharova et al., 1996), desorption kinetics of radionuclides, which at the adsorption stage form strong chemical bounds with elements of crystal lattice, is controlled by “the mechanisms of leaching”. The possibility of forming this type of chemical bonds is associated with the manifestation of specific adsorption as established during a study of sandy cores at a radioactively contaminated site (Pickens et al., 1981; Jackson and Inch, 1983). Experimental data showed that up to 15% of Sr-90 is held by a sediment in the specifically adsorbed (by hydroxides of iron and aluminum) state, and a strong correlation was established between the release of the residual Sr-90 and content of extractable Fe, Al and Mn from the sediment.

In a number of experiments with radionuclides, however, only slight discrepancies between the sorption and desorption coefficients were detected (Aksoyoglu et al., 1990). Moreover, some researchers treat the hysteresis as an artifact; that is, the noncoincidence of the adsorption and desorption distribution coefficients is explained by a nonequivalence of experimental conditions at the stage of adsorption and desorption; or by not reaching the state of equilibrium in the system (Ma and Selim, 1994; Streck et al., 1995) when the kinetically expressed process is interpreted within the framework of equilibrium models. As it was correctly noted by Lyon and Patterson (1984) who studied the nonequilibrium of Sr-90 adsorption/desorption, some of the radionuclides, which cannot be desorbed in short-term laboratory experiments can be removed over a period of 10–15 years in a groundwater flow system.

This study was motivated by the authors' investigations being conducted at the Pilot Site for Deep-Well Injection of Radioactive Wastes in Western Siberia, Russia (Rybalchenko, 1998). The site is associated with two systems of injection wells, which are used for disposal of low (LLW) and intermediate (ILW) level radioactive wastes in a deep geological formation. The (discharge) injection flow rate varies from 200 (ILW) to 3000 (LLW) m³ day⁻¹, and the total activity of the waste varies from 3.7×10⁴ to 3.7×10⁸ Bq l⁻¹ (pH about 3).

The injection of intermediate level radioactive wastes in a deep geological formation at the site is accompanied by heat evolution. The temperature of the formation rises to more than 100 °C. That is why the behavior of radionuclides in the subsurface environment is studied with batch laboratory experiments, which have been conducted under elevated temperature ($T=70$ °C) and pressure ($P=3$ MPa) conditions. This pressure corresponds to an overburden of about 300 m. These experimental results are compared with data previously obtained under room conditions ($T=20$ °C and $P=0.1$ MPa).

During a natural attenuation period which is expected to start when the injection of the waste is stopped and the contaminants are supposed to be flushed out of pores by fresh

water, the desorption process will play a dominating role in transport of the waste. Thus, an experimental study of desorption is of special interest for determining long-term impacts of the waste.

The purposes of this study are (1) to identify principal mechanisms responsible for adsorption hysteresis under different geochemical, temperature and pressure conditions; (2) to develop analytical and numerical models which take into account (a) microscopic heterogeneity of multimineral aquifers, and (b) variations of an external chemical potential resulting from the rate-limited transformations of the mineral phase; and (3) to demonstrate how the latter processes may affect the mobility of the radionuclides in the subsurface environment.

2. Materials, methods and experimental series

For studying adsorption/desorption processes, several series of laboratory batch experiments with Sr-90 and Cs-137 were performed. The experiments differ in (a) radionuclide composition of the liquid phase, (b) composition of the solutions used in adsorption and desorption stages of the experiments, (c) temperature/pressure regime of the experiments.

The liquid phase for the adsorption stage was represented by a synthesized groundwater (Table 1) or an acid (pH 3) solution of NaNO_3 (10 g l^{-1}), which includes the following cations of three and bivalent metals (g l^{-1})— Ni^{3+} : 0.33, Cr^{3+} : 0.86, Mn^{2+} : 0.30.

Desorption of previously adsorbed radionuclides was performed using the same solution of sodium nitrate, or the synthesized groundwater. The temperature between experiments was varied from 20 to 70 °C. Pressure steps were varied between 0.1 and 3 MPa. Thus, a wide range of conditions were simulated in the laboratory, which correspond to different stages of the migration processes in groundwater.

Rock samples were taken from a potentially contaminated aquifer. A geosorbent (aquifer material) is defined by a mixture of different lithological types of the rock (an “average sample”). The artificially prepared mixture contains minerals (Table 2), which differ in adsorption properties, as well as minerals that potentially dissolve in acid solutions.

Each of the laboratory experiment used 1 or 2 g samples of rock (previously conditioned using a synthesized groundwater), of mass, m_s . The volume of the solution (V) was 10 or 20 ml, so the volume to weight/mass ratio was 10 in all experiments ($V/m_s=10$).

In the setup of the laboratory tests, the kinetic stages of the adsorption and multistep desorption of the radionuclides Cs-137 and Sr-90 were controlled reliably.

Solutions were detected by HPGe-MCA gamma counting system and beta scintillation counting of Sr/Y to determine cesium-137 and strontium-90 concentrations. Water

Table 1
Chemical composition of groundwater (a major horizon for the radioactive waste disposal)

Anions (mg/l)					Cations (mg/l)			pH
CO_3^{2-}	HCO_3^-	NO_3^-	SO_4^{2-}	Cl^-	Na^+	Ca^{2+}	Mg^{2+}	
1.49	234	0.6	2.47	6.43	111.2	3.7	0.6	7.6–8.0

Table 2
Mineralogy composition of the rock

No.	Mineral	Lab data (% mass)	Type of reactive sites
1	Plagioclase	2.6	1
2	Biotite	7.6	2
3	Hydromica	11.7	2
4	Montmorillonite	11.4	2
5	Quartz	63	1
6	Carbonates	1.1	1
7	Rutile	0.3	1
8	Pyrolusite	0	1
9	Total mass of mineral phase (g)	98.04	

samples were analyzed by atomic adsorption spectrometry for cations that might compete with radionuclides for adsorption sites. pH measurements were made with a combination electrode.

For an identification of the adsorption and desorption isotherm (type of graph in the coordinates N^S/N^d versus C , where N^S and N^d are the concentrations of radionuclide in the solid phase at adsorption/desorption stages, C is the radionuclide concentration in solution), several initial concentrations (C_i) of radionuclides were used; the test concentration range was $3.7 \times (10^5 - 10^8)$ Bq l^{-1} . These concentrations were close to the concentrations detected in the radioactive waste. The concentration in the solid phase ($N^{S/d}$) was normalized to the volume of the rock (the bulk density of rock and groundwater, ρ_n , was assumed to be 1.7 g cm^{-3}).

The composition of the solutions used for the adsorption and desorption experiments and pressure and temperature conditions are summarized in Tables 3 and 4. The indices for the experimental series are explained in the notes for Table 3.

Table 3
Laboratory series (at $T=20 \text{ }^\circ\text{C}$ and $P=P_{\text{atm}}$)

Radionuclide	Solutions			
	Adsorption		Desorption	
	Groundwater	NaNO ₃	NaNO ₃	Groundwater
Sr-90	Sr-GW	Sr-Na	Sr-Na-Na	Sr-Na-GW, Sr-GW-GW
Cs-137	–	Cs-Na	Cs-Na-Na	Cs-Na-GW

Note (experimental series indexes):

GW and Na means ground water and sodium nitrate solution, Sr-GW: adsorption of radiostrontium in groundwater solution.

Sr(Cs)-Na: adsorption of Sr-90 (Cs-137) in sodium nitrate solution.

Sr(Cs)-Na-Na: adsorption Sr-90 (Cs-137) in sodium nitrate solution and desorption under the same condition (environment).

Sr(Cs)-Na-GW: adsorption of Sr-90 (Cs-137) in sodium nitrate solution and desorption under the ground water condition.

Sr-GW-GW: adsorption and desorption of Sr-90 in the ground water.

3. Results: qualitative analysis

3.1. Variations in the main component composition and pH of the solution

Monitoring the concentration change of major components in the liquid phase during the process of multistep flushing of the rock samples by the acid sodium nitrate solution indicates (Fig. 1a) that the first interaction of the rock and solution results in a sharp rise in the calcium ion concentration (up to 100 mg l^{-1}), magnesium (up to 50 mg l^{-1}), strontium (up to 4.8 mg l^{-1}) and potassium ions (up to 7.9 mg l^{-1}). These concentrations significantly exceed (up to one to two orders of magnitude) the background concentrations of the components in the formation water (Table 1) as well as in the flushing solution. Apparently, at this stage, an active dissolution of carbonate minerals and displacement of cations from exchange complex occur. The subsequent iterations (incubation periods) are characterized by a decrease in concentrations of the cations in the solution. Thus, the multistep interactions between the solid and liquid phases leads to a reserves depletion of dissolving salts (minerals) and to a redistribution of the exchanging cations in the system. In addition, the process may be accompanied by an alteration of silica (first of all mica) minerals. The “acid–alkaline” reaction of the solution changes slightly (pH from 3.05 to 3.20).

A system response to a substitution of the acid solution at the first and subsequent desorption steps for the synthesized (“fresh”) groundwater (Fig. 1b) is as follows: a rather quick (two desorption steps) removal from the system occurs for practically all of the major cations (Ca^{2+} , Mg^{2+} , Fe^{3+}) as well as stable strontium (Sr^{2+}). The potassium-ion concentration (K^+) decreases more slowly. Of the cations which were present in the solution before flushing of the rock by the synthesized water, only sodium ions remain in

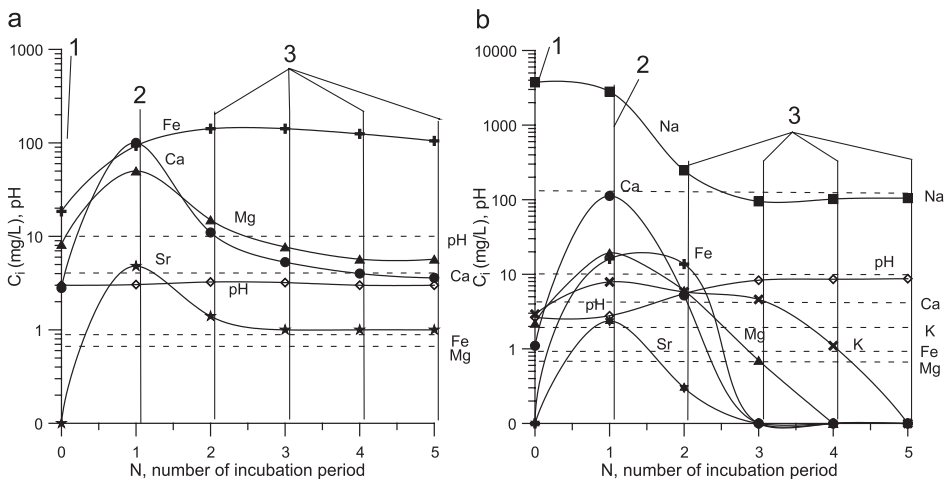


Fig. 1. A change in the major component composition of solution, which was measured in the multistep flushing of the rock by solution of NaNO_3 (a) and groundwater (b). Dotted lines show the initial composition of groundwater. (1) Displacing solution (NaNO_3 , before the adsorption step), (2) equilibrium at the adsorption step, (3) equilibrium at the desorption steps.

the system at concentrations near background. During desorption, the pH of the solution increases dramatically from 2.8 to 8.7.

3.2. Kinetics of the process

3.2.1. Experiments under atmosphere pressure and temperature 20 °C

An analysis of the kinetic curves (Fig. 2a and b) shows that in general adsorption/desorption can be considered as a transient (or nonequilibrium) process. In 7–10 days after

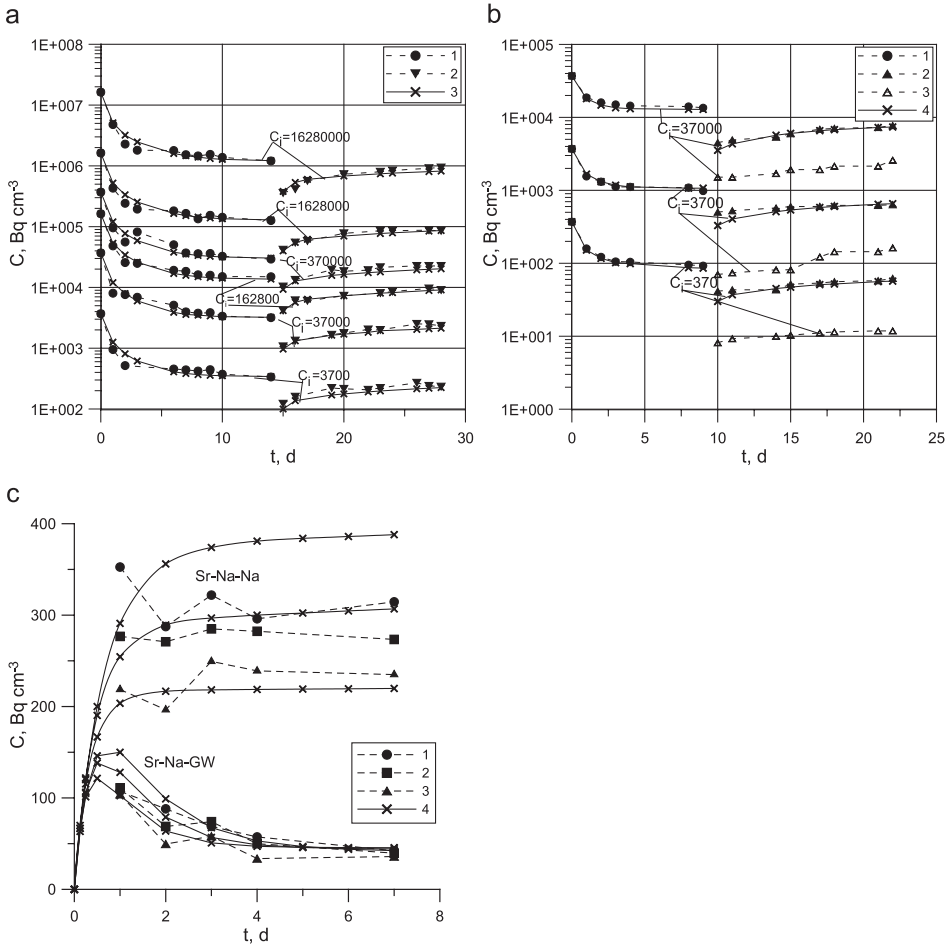


Fig. 2. Kinetic (experimental and predicted) curves of adsorption and desorption (first step) periods. (a) Series Sr-GW-GW [(1) adsorption, experimental data; (2) desorption, experimental data; (3) fitted curves]. (b) Cs-Na-Na and Cs-Na-GW [(1) adsorption under NaNO₃ environment, (2) desorption under NaNO₃ environment, (3) adsorption under GW environment, (4) modeling curves for Cs-Na-Na series]. (c) Desorption of Sr-90, series Sr-Na-Na and Sr-Na-GW [(1) $C_i=3700$ Bq cm⁻³, (2) $C_i=37,000$ (scale 1/10) Bq cm⁻³, (3) $C_i=370,000$ (scale 1/100) Bq cm⁻³, (4) modeling curves]. C_i (Bq cm⁻³) is the concentration of the radionuclide in the solution at the adsorption step.

the beginning of the experiments, however, the process tends to reach equilibrium. No anomalous effects are observed. A period of 1–2 weeks is probably sufficient to reach a state of near equilibrium for the given experimental conditions.

Kinetic desorption curves in the experimental series Sr-Na-GW display an anomalous nature (Fig. 2c). This was the case when Sr-90, which was adsorbed from the sodium nitrate solution, was washed out by fresh water. The desorption of a radionuclide, which is dominating at the beginning of the interaction between the contaminated porous material and water, becomes negligible in comparison with adsorption dominating at the latest periods. This is in contrast to the expected increase of the radionuclide concentration in the solution.

The fitting of the data points with curves in Fig. 2 is discussed in Section 5.1.

3.2.2. Experiments under elevated temperature and pressure

The first set of experimental series with radionuclides (Sr-Na-GW-70, Cs-Na-Na-70 and Cs-Na-GW-70) (Table 4) was carried out at the temperature 70 °C and under normal atmospheric pressure ($P=P_{\text{atm}}$). Another set of experiments (Sr-Na-GW-70-3, Cs-Na-Na-70-3 and Cs-Na-GW-70-3) was carried out at the same temperature, but at a pressure of 3 MPa.

3.2.2.1. $T=70\text{ }^{\circ}\text{C}$ and $P=P_{\text{atm}}$. At the sorption step of the experimental series with Sr-90, rather slow changes of the concentration function, C , were noted (Fig. 3a–c). This suggests that the process is affected by a dissolution of carbonate minerals and/or a hydrolysis of alumina silicates. In the desorption kinetic curves, the extremes that were noted under room conditions (Section 3.2.1) could not be observed. Adsorption curves obtained for Cs-137 with hot and cold acid solutions (Fig. 3d–f) did not differ much from each other. One may anticipate that the mineral dissolution produces ions which did not compete for the adsorption sites with Cs-137.

3.2.2.2. $T=70\text{ }^{\circ}\text{C}$ and $P=3\text{ MPa}$. Breakthrough curves obtained at the adsorption stage of the experiments with NaNO_3 solution have shown a nonmonotonic nature (Fig. 3). During the first days from the beginning of the experiments, a drop in radionuclide concentration in the NaNO_3 solution was observed. At later times, however, an increase in the radionuclide content in the solution was noted. This effect is most pronounced for Sr-90: its concentration at the end of the sorption experiment (14 days) reaches the initial values (Fig. 3a–c). This means that Sr-90 was adsorbed at first by the rock in large quantities. Then it was completely desorbed into the solution, so that the rock was clean of the contaminants.

Table 4

Laboratory series (experiments under elevated temperature/pressure conditions)

Radionuclide	Temperature/pressure condition	
	$T=70\text{ }^{\circ}\text{C}$, $P=P_{\text{atm}}$	$T=70\text{ }^{\circ}\text{C}$, $P=3\text{ MPa}$
⁹⁰ Sr		
Desorption by GW	Sr-Na-GW-70	Sr-Na-GW-70-3
¹³⁷ Cs		
Desorption by NaNO_3	Cs-Na-Na-70	Cs-Na-Na-70-3
Desorption by GW	Cs-Na-GW-70	Cs-Na-GW-70-3

Radionuclide adsorption took place in sodium nitrate solution environment.

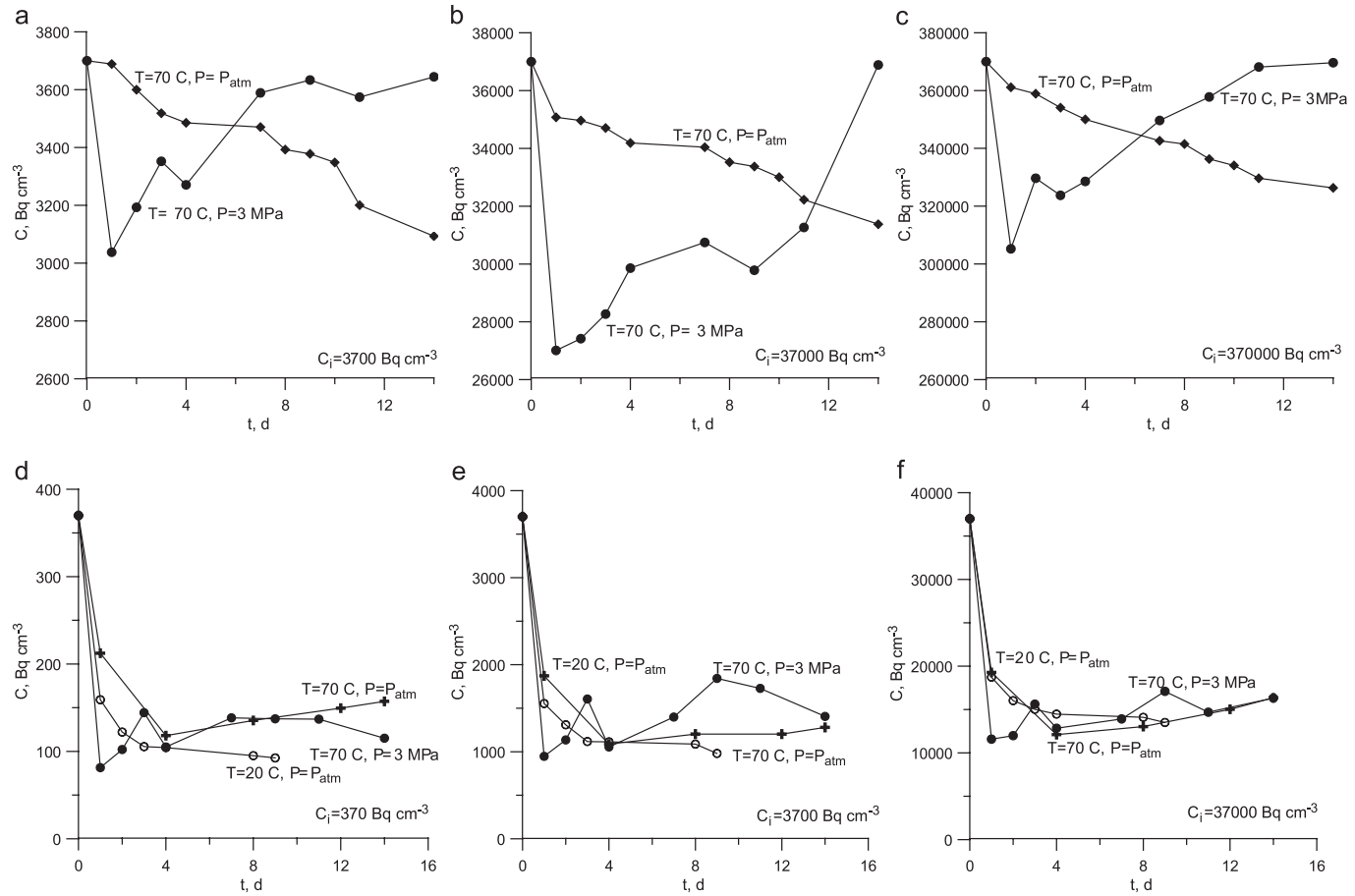


Fig. 3. Influence of the temperature and pressure on radionuclide adsorption kinetics: (a, b and c) Sr-90 adsorption [(a) C_i=3700 Bq cm⁻³, (b) C_i=37,000 Bq cm⁻³, (c) C_i=370,000 Bq cm⁻³]; (d, e and f) Cs-137 adsorption [(d) C_i=370 Bq cm⁻³, (e) C_i=3700 Bq cm⁻³, (f) C_i=37,000 Bq cm⁻³].

The calculated apparent constant of the sorption distribution is supposed to be equal to zero (i.e., a release of Sr-90 is about 100%). A release of Cs-137 reaches 15–20%.

The phenomenon established experimentally can be explained if we take into account that adsorption equilibrium is controlled by dissolution kinetics of minerals in the solid phase. Indeed, adsorption and desorption are sufficiently rapid processes compared with mineral dissolution. Therefore, Sr-90 is actively adsorbed at first, when the solution is undersaturated by competing bivalent cations (principally, calcium). Later, however, the concentration of these cations gradually increases, due to dissolution of carbonate minerals. This leads to a release of Sr-90 from the exchange complex of the rock. The degree of solution saturation by calcium ions is proportional to the concentration (partial pressure) of carbon dioxide, whose solubility rises with a pressure increase. Therefore, at the elevated pressure, calcium concentration can reach values which indicate that practically all Sr-90 has been released to the solution.

At elevated temperature and pressure, the acid solution of NaNO₃ can also dissolve some silicate minerals, e.g., hydro-mica. In this case, the solution must be enriched gradually with potassium ions that compete with Cs-137 for the exchange positions on the matrix. Therefore, it can be supposed that an accumulation of potassium ions in the solution leads to the release of previously adsorbed Cs-137 (series Cs-Na- Na/GW-70-3, Fig. 3d–f).

3.3. Equilibrium relationships and isotherms

3.3.1. Adsorption and desorption isotherms

The best fit of the log-transformed experimental data (Figs. 4–6) characterizing adsorption equilibrium is a line. It means that adsorption isotherms are of the Freundlich type:

$$N^s = K_F^S C^{n^s} \text{ or } \ln N^s = \ln K_F^S + n^s \ln C, \quad (1)$$

where C is the equilibrium concentration in the solution, N^s is the concentration on the solid phase at the adsorption stage of the experiment, K_F^S , and n^s are the linear and exponential Freundlich constants respectively, and s is sorption (forward reaction).

An analysis of the experimental results shows that with a few exceptions all desorption concentration points are located above the adsorption isotherms: that is, desorption isotherms do not coincide with adsorption isotherms (Figs. 4–6). The experimental data display a hysteresis in the adsorption process. Probably, a new chemical equilibrium is reached at each of the desorption steps. In this case, a line connecting the measured points $C-N$ can be considered as a desorption isotherm. An analysis of the experimental results indicates that the desorption process can be described by the Freundlich relationship as well:

$$N^d = K_F^d C^{n^d} \text{ or } \ln N^d = \ln K_F^d + n^d \ln C, \quad (2)$$

where N^d is the concentration in the solid phase at the desorption stage, K_F^d , and n^d are the linear and exponential constants for desorption respectively, and d is desorption (backward reaction). At the same time, there are some deviations of the experimental measurements from Eq. (2) caused by the irreversibility of adsorption.

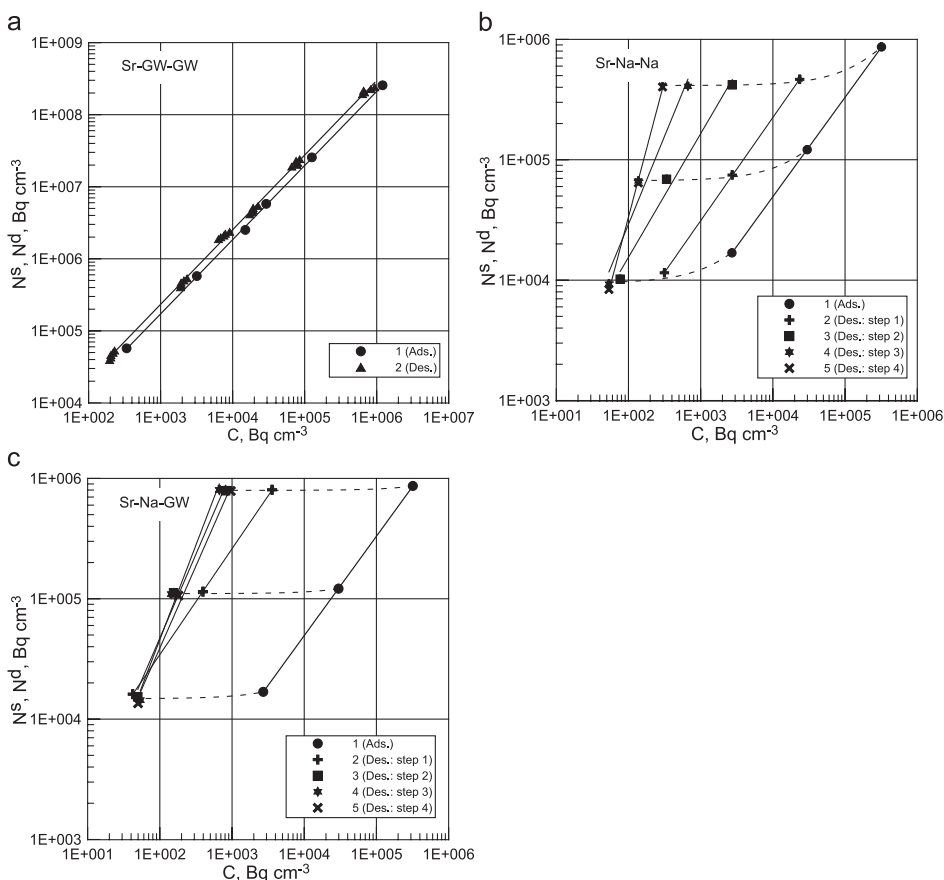


Fig. 4. Isotherms of adsorption and desorption of Sr-90 (double-log scale) for experimental series. (a) Sr-GW-GW [(1) adsorption, fitting curve: $N^s=140.7C^{1.03}$, (2) desorption, fitting curve: $N^d=183.5C^{1.04}$]. (b) Sr-Na-Na [(1) adsorption: $N^s=24.6C^{0.83}$, (2) desorption, step 1: $N^d=83.4C^{0.86}$, (3) desorption, step 2: $N^d=136.9C^{1.03}$, (4) desorption, step 3: $N^d=34.4C^{1.57}$, (5) desorption, step 4: $N^d=1.0C^{2.26}$]. (c) Sr-Na-GW [(1) adsorption: $N^s=24.6C^{0.83}$, (2) desorption, step 1: $N^d=598.2C^{0.88}$, (3) desorption, step 2: $N^d=77.0C^{1.39}$, (4) desorption, step 3: $N^d=33.0C^{1.57}$, (5) desorption, step 4: $N^d=72.6C^{1.36}$].

3.3.2. Experiments under atmosphere pressure and temperature 20 °C

3.3.2.1. *Strontium-90*. In the system with synthetic groundwater (Sr-GW-GW), the adsorption and desorption isotherms do not differ much (Fig. 4a, Table 5). A minor divergence of the two stages of the experiments can be explained by kinetics of the process. The presence of the dissolved sodium nitrate and products of its interaction with the mineral phase in the solution decreases the adsorption capacity of the rock, resulting in a nonlinear process (n^s is less than 1) (Fig. 4b, Table 5).

The observed adsorption–desorption hysteresis (Fig. 4b,c) can result from variations of the major cation content and pH. Thus, the chemical equilibrium at the first desorption step is characterized by the presence of a noticeably smaller amount of the displaced cations in

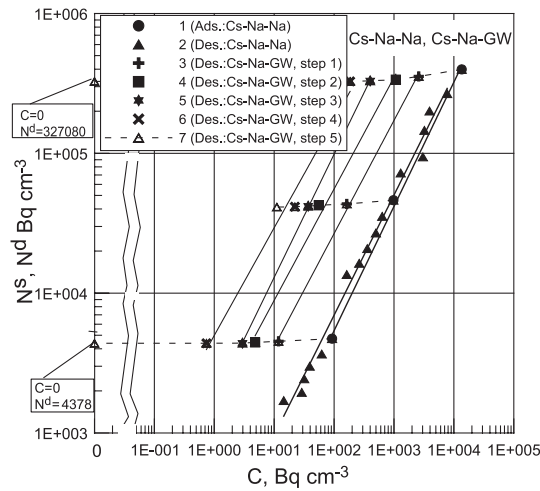


Fig. 5. Isotherms of Cs-137 adsorption and desorption (double-log scale). Experimental series Cs-Na-Na and Cs-Na-GW: (1) adsorption (NaNO₃ environment: $N^s=90.0C^{0.89}$); (2) desorption in NaNO₃: $N^d=133.0C^{0.86}$; (3) desorption in SGW: 1 step, $N^d=642.3C^{0.81}$; (4) desorption in SGW: 2 steps, $N^d=1417.9C^{0.80}$; (5) desorption in SGW: 3 steps, $N^d=1706.0C^{0.88}$; (6) desorption in SGW: 4 steps, $N^d=4982.2C^{0.77}$; (7) desorption in SGW: 5 steps.

the solution, compared with the adsorption stage. Therefore, the equilibrium condition differs from the condition occurring at the adsorption stage. The same tendency is also seen in the subsequent desorption steps, which are characterized by a gradual decrease of cations of alkali earth metals from the system. Although the desorption equilibrium is described by the same type of isotherm (Fig. 4b) the values of K_F^d and n^d parameters in Eq. (2) change from one step to the next (Table 5).

When desorption takes place in synthetic groundwater (series Sr-Na-GW), Sr-90 releases less readily from the reactive (adsorption) sites compared with desorption into the acid solution of NaNO₃. Therefore, the residual concentration of Sr-90 on the rock (N^d) is higher than in series Sr-Na-Na (Fig. 4c). The first desorption isotherm is characterized by a

Table 5
Freundlich adsorption–desorption constants from the batch experiments

Stage of the experiment	Sr-90						Cs-137				
	Sr-GW-GW		Sr-Na-Na		Sr-Na-GW		Cs-Na-Na		Cs-Na-GW		
	$K_F^{s/d}$	$n^{s/d}$	$K_F^{s/d}$	$n^{s/d}$	$K_F^{s/d}$	$n^{s/d}$	$K_F^{s/d}$	$n^{s/d}$	$K_F^{s/d}$	$n^{s/d}$	
Adsorption	141	1.03	24.6	0.83	24.6	0.83	90.6	0.89	90.6	0.89	
Desorption (step number)	1		83.4	0.86	598	0.88			642	0.81	
	2		137	1.03	77.0	1.39			1418	0.80	
	3	183.5	1.04	34.4	1.46	33.0	1.57	133	0.86	1706	0.88
	4			1.0	2.26	72.6	1.36			4982	0.77
	5			ND	ND	ND	ND			IRA	

ND: no data, IRA: irreversible adsorption; $K_F^{s/d}$, $n^{s/d}$: linear and exponential Freundlich adsorption/desorption constants.

coefficient n^d , which is close to its adsorption coefficient n^s ; the value for K_F^d rises because the solution is of a much lower ionic strength than before the desorption step (Table 5). As in the preceding case, further desorption steps lead to an increase in the constant n^d and a drop in the values of the coefficient K_F^d .

3.3.2.2. *Cesium-137*. The sorption ability of Cs-137 is higher than that of Sr-90: K_F^s (series Cs-Na) \gg K_F^s (series Sr-Na), Table 5. However, a decrease in the saturation of the solution by cations of alkali-earth metals at the desorption steps in the experimental series

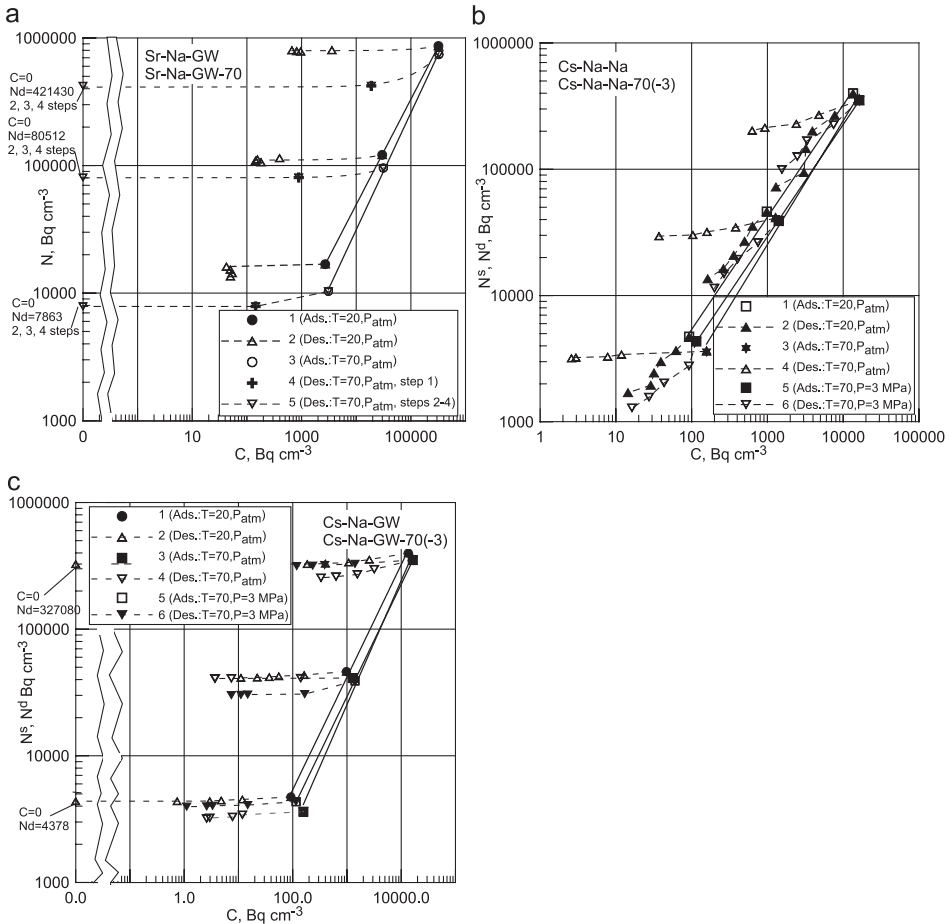


Fig. 6. Influence of the temperature and pressure on adsorption and desorption isotherms. Experimental series: (a) Sr-Na-GW [(1) adsorption: $T=20\text{ }^{\circ}\text{C}$, $P=P_{\text{atm}}$; (2) desorption: $T=20\text{ }^{\circ}\text{C}$, $P=P_{\text{atm}}$; (3) adsorption: $T=70\text{ }^{\circ}\text{C}$, $P=P_{\text{atm}}$; (4) desorption: $T=70\text{ }^{\circ}\text{C}$, $P=P_{\text{atm}}$, step 1; (5) desorption: $T=70\text{ }^{\circ}\text{C}$, $P=P_{\text{atm}}$ (2, 3, 4 steps)]. (b) Cs-Na-Na [(1) adsorption: $T=20\text{ }^{\circ}\text{C}$, $P=P_{\text{atm}}$; (2) desorption: $T=20\text{ }^{\circ}\text{C}$, $P=P_{\text{atm}}$; (3) adsorption: $T=70\text{ }^{\circ}\text{C}$, $P=P_{\text{atm}}$; (4) desorption: $T=70\text{ }^{\circ}\text{C}$, $P=P_{\text{atm}}$; (5) adsorption: $T=70\text{ }^{\circ}\text{C}$, $P=3\text{ MPa}$; (6) desorption: $T=70\text{ }^{\circ}\text{C}$, $P=3\text{ MPa}$]. (c) Cs-Na-GW [(1) adsorption: $T=20\text{ }^{\circ}\text{C}$, $P=P_{\text{atm}}$; (2) desorption: $T=20\text{ }^{\circ}\text{C}$, $P=P_{\text{atm}}$; (3) adsorption: $T=70\text{ }^{\circ}\text{C}$, $P=P_{\text{atm}}$; (4) desorption: $T=70\text{ }^{\circ}\text{C}$, $P=P_{\text{atm}}$; (5) adsorption: $T=70\text{ }^{\circ}\text{C}$, $P=3\text{ MPa}$; (6) desorption: $T=70\text{ }^{\circ}\text{C}$, $P=3\text{ MPa}$].

Cs-Na-Na in Fig. 5, does not lead to a retention of Cs-137 in the solid phase. Very likely, the equilibrium in the system is controlled exclusively by the ionic strength of the solution, which changes slightly from one desorption step to the next.

A step-by-step washout of the contaminated rock with the synthesized groundwater (series Cs-Na-GW) leads to a displacement of the desorption isotherms along the concentration axis C with respect to the adsorption line (Fig. 5). In contrast to the previous experiments, however, the desorption isotherms remain approximately parallel to the adsorption isotherm up to the fourth desorption step: the linear coefficient K_F^d increases considerably, while the exponential index n^d changes only slightly (Table 5). Flushing the rock samples, which were contaminated at the adsorption stage, with fresh water did not result in a release of a detectable amount of Cs-137 from the mineral phase after five washes (Fig. 5).

3.3.3. Experiments under elevated temperature and pressure

3.3.3.1. $T=70\text{ }^\circ\text{C}$ and $P=P_{atm}$. Experimental data and models characterizing the equilibrium of the system are presented in Fig. 6 and Table 6. A rise of the solution temperature resulted in an apparent decrease of the capacity of the porous medium to adsorb radionuclides. Furthermore, an increase in the temperature of the system resulted in more linear sorption. This behavior is explained in Section 3.2.2. An increase in the temperature leads to a more intensive dissolution of carbonate and silicate minerals. Therefore, the solution at higher temperature is characterized by greater concentrations of the bivalent cations of alkaline earth metals than at $T=20\text{ }^\circ\text{C}$. These ions compete with the Sr-90 for adsorption sites, thereby causing faster dissolution at $T=70\text{ }^\circ\text{C}$.

A further analysis of a batch experiment with Sr-90 (Sr-Na-GW-70) demonstrated that a rise in the temperature caused an irreversibility of the sorption process (Fig. 6a). Starting with the second desorption step, the solution loses radioactivity completely ($C=0$). The radionuclide could not be removed from the exchanged complex of the rock due to a strong deficiency of bivalent cations in the solution, which resulted from the first interaction of the rock with the hot acid solution. In contrast to the series Cs-Na-Na ($T=20\text{ }^\circ\text{C}$), no irreversibility of the Cs-137 adsorption was noted in the experimental series Cs-Na-GW-70 (Fig. 6b).

3.3.3.2. $T=70\text{ }^\circ\text{C}$ and $P=3\text{ MPa}$. The measured amount of Sr-90 in the solid phase at the end of the adsorption experiments is close to zero. The results of the adsorption experiments with Cs-137 under the same conditions were close to the experiments with the

Table 6
Fitting equilibrium adsorption constants

Radionuclide (experimental series)	$T=20\text{ }^\circ\text{C}, P=P_{atm}$		$T=70\text{ }^\circ\text{C}, P=P_{atm}$		$T=70\text{ }^\circ\text{C}, P=3\text{ MPa}$	
	K_F^s	n^s	K_F^s	n^s	K_F^s	n^s
Sr-90 (Sr-GW)	140.7 (cm ³ /Bq) ^{0.03}	1.03	ND		ND	
Sr-90 (Sr-Na)	24.6 (cm ³ /Bq) ^{-0.17}	0.83	6.7 (cm ³ /Bq) ^{-0.08}	0.92	NS	
Cs-137 (Cs-Na)	90.0 (cm ³ /Bq) ^{-0.11}	0.89	29.1 (cm ³ /Bq) ^{-0.02}	0.98	63.8 (cm ³ /Bq) ^{-0.11}	0.89

ND: No data, NS: No sorption.

hot solution conducted under atmospheric pressure. The relevant adsorption isotherms in Fig. 6b and c practically coincide. As seen in Fig. 6b, the desorption points deviated less from the adsorption isotherm (desorption into the NaNO₃ solution, series Cs-Na-Na-70-3) than what was observed in the experiment at $T=70$ °C and $P=P_{\text{atm}}$ (series Cs-Na-Na-70). The desorbed amount of Cs-137 in series Cs-Na-GW-70-3 is almost the same as in previous series Cs-Na-GW-70 (Fig. 6c).

4. Description of the models

Depending on the experimental series, two alternative models can be applied for interpretation of the laboratory tests: (1) a nonequilibrium model of dual-site one-component adsorption and (2) a one-site kinetic model of adsorption with concomitant mineral dissolution.

4.1. Nonequilibrium model of dual-site one-component adsorption

A number of publications (Selim and Amacher, 1988; Jackson and Inch, 1989; Van Genuchten and Wagenet, 1989; Ma and Selim, 1994; Streck et al., 1995; Huang et al., 1998; Weber et al., 1998; Rumynin et al., 2002) address the kinetic modeling of heterogeneous sorption sites and support the hypothesis of sorption/desorption hysteresis. For example, such a model has effectively been used to describe the hysteresis in adsorption of water-soluble hydrophobic organic compounds (pesticides—phenanthrene, simazine and atrazine) on soils (Ma and Selim, 1994; Streck et al., 1995; Huang et al., 1998; Weber et al., 1998). These works explained the hysteresis by a low desorption rate and the heterogeneity of the sorption properties of the natural organic matter.

An initial hypothesis is based on the assumption that two types (i.e., types 1 and 2) of reactive sites exist in a representative volume of the porous media. These two types of sites differ in equilibrium and kinetic parameters controlling interactions between components presented in the liquid and solid phases.

If the adsorption process is under the conditions of a local equilibrium and obeys the Freundlich isotherm [Eq. (1)], then the adsorption kinetics on the two types of the reactive sites can be described as follows:

$$f \frac{dN_1}{dt} = \alpha_1^s \left(K_{F_1}^s C^{n_1^s} - N_1 \right),$$

$$(1 - f) \frac{dN_2}{dt} = \alpha_2^s \left(K_{F_2}^s C^{n_2^s} - N_2 \right), \quad (3)$$

where C is the concentrations of the radionuclide in solution, N_1 and N_2 are concentrations on the rock (for type 1 and type 2 sites, respectively), $K_{F_1}^s$ and $K_{F_2}^s$ are the partial linear Freundlich constants, n_1^s and n_2^s are the partial exponential constants, α_1^s and α_2^s are the kinetic adsorption constants, f is the fraction of the site 1 (corresponding to a portion of the first type of the sites within the porous matrix).

The corresponding equations for the desorption are as follows:

$$f \frac{dN_1}{dt} = \alpha_1^d \left(K_{F_1}^d C^{n_1^d} - N_1 \right)$$

$$(1-f) \frac{dN_2}{dt} = \alpha_2^d \left(K_{F_2}^d C^{n_2^d} - N_2 \right). \quad (4)$$

Eq. (5) describes the mass balance in a batch experiment:

$$\frac{dM^T}{dt} = 0, M^T = VC + N(m_s/\rho_b), \quad (5)$$

where V is the volume of the solution, m_s is the weight of the rock sample, ρ_b is the bulk density, N is the total radionuclide concentration in the solid phase:

$$N = fN_1 + (1-f)N_2. \quad (6)$$

The system [Eqs. (3)–(6)] is closed when the initial conditions ($t=0$) are assumed as follows:

$$N_1 = N_2 = 0, C = C_i \text{ at the adsorption stage,}$$

$$N_1 = N_{i1}, N_2 = N_{i2}, C = 0 \text{ at the desorption stage,} \quad (7)$$

where C_i is the initial concentration of the adsorbing component in the solution, N_{i1} and N_{i2} are the initial concentrations of the component on the sorption sites upon substitution of the solution.

For solving the system of the differential Eqs. (3) (4) (5) and (6), a numerical algorithm using a finite difference solution method was developed.

4.2. One-site kinetic model of adsorption with concomitant mineral dissolution

An influence of the cations, which are present in the solution in “macroquantities”, on the adsorption of Sr-90 and Cs-137 was observed in numerous previous experiments (e.g., Klechkovsky and Gulyakin, 1958; Kokotov and Popov, 1962; Liszewski et al., 1998; EPA, 1999). These experiments used prepared solutions, which initially contained cations of the mentioned bivalent metals. In this section, we show how variations in main component concentrations resulting from the rate-limited dissolution of the mineral phase can affect the kinetically controlled adsorption and desorption.

4.2.1. Physical assumptions and solution of the base equation

Assumptions of the analysis provided in this section are that (1) the adsorption process is an ion-exchange, (2) mineral dissolution produces cations that compete for adsorption (ion exchange) sites with a radionuclide, (3) radionuclide concentrations on a mineral phase are much lower than those of the total exchange capacity (Q_v), (4) the solution of NaNO_3 is a

buffer, and, therefore, a minor change of the sodium concentration affects only weakly the equilibrium between radionuclide and competing Na^{2+} .

In accordance with the law of mass action, the ion-exchange equilibrium in the two-component system is determined by Eq. (8) (Charbeneau, 1982):

$$K_{12} = \left(\frac{N_1}{C_1} \right)^{z_2} \left(\frac{C_2}{N_2} \right)^{z_1}, \quad (8)$$

where C_1 and C_2 are the concentrations of the displacing cation of radioactive metal (1) and of the displaced cation of stable component in the solution (2), respectively; N_1 and N_2 are the concentrations of radionuclide and stable component on solid surfaces, respectively; K_{12} is the selectivity coefficient for the cation-exchange reaction between 1 and 2; and z_1 and z_2 are the corresponding charges of cations.

Assuming $Q_v = N_1 + N_2$ and $N_1 \ll N_2$ (i.e., that the concentration of radionuclides on the solid phase is significantly smaller than the concentration of the displaced cation), Eq. (8) becomes:

$$N_1 = \frac{C_1}{K_s C_2^{\bar{z}}}, \quad (9)$$

where $\bar{z} = z_1/z_2$, $K_s = (K_{12} Q_v^{z_1})^{-1/z_2}$.

The validity of these assumptions and Eq. (9) was confirmed experimentally during a study on the influence of calcium ions on the calculated values of the Sr-90 distribution coefficient (K_d) (Yegorov et al., 1961; Kokotov and Popov, 1962). A strong inverse linear relationship between the adsorbed strontium and calcium+magnesium concentrations in solution was also noted in experimental work by Liszewski et al. (1998).

In this case, the equation describing the adsorption kinetics can be written in a form:

$$\frac{dN_1}{dt} = \alpha_1 (C_1 - K_s C_2^{\bar{z}} N_1), \quad (10)$$

where α_1 is the kinetic constant.

A mass balance equation for the construction of a model for batch experiment interpretation is as follows:

$$\frac{dM^T}{dt} = 0, \quad M^T = V C_1 + N_1 (m_s / \rho_b) \quad (11)$$

or

$$a \frac{dC_1}{dt} + \frac{dN_1}{dt} = 0, \quad (12)$$

where V is the volume of the solution, m_s is the weight of the rock sample, ρ_b is the bulk density, and $a = V \rho_b / m_s$.

The radionuclide concentration on the solid phase (N_1) for two phases of the experiment (adsorption and desorption) can be presented as follows:

$$N_1 = a(C_1^0 - C_1) \text{ for adsorption, and} \quad (13)$$

$$N_1 = N_0 - aC_1 \text{ for desorption,} \quad (14)$$

where C_1^0 is the initial (before the sorption step) radionuclide concentration in the solution, $N_0 = a(C_1^0 - C_1^*)$ is the concentration of the radionuclide on the rock before desorption, C_1^* is the concentration which was measured at the end of the adsorption step.

Substituting Eqs. (12), (13) and (14) into the kinetic Eq. (10), we obtain the following equations:

$$\frac{dC_1}{dt} = \alpha_1 \left[K_s C_2^{\bar{z}} C_1^T - \left(\frac{1}{a} + K_s C_2^{\bar{z}} \right) C_1 \right], \text{ for adsorption} \quad (15)$$

$$\frac{dC_1}{dt} = \alpha_1 \left[K_s C_2^{\bar{z}} \frac{N_0}{a} - \left(\frac{1}{a} + K_s C_2^{\bar{z}} \right) C_1 \right], \text{ for desorption} \quad (16)$$

Considering a dissolution reaction that proceeds in parallel to the sorption reaction and which is presented by a first-order rate equation (Golubev, 1981):

$$C_2 = C_2^H - (C_2^H - C_2^0) e^{-\alpha_2 t}, \quad (17)$$

where C_2^0 is the initial concentration of the cation in the solution, C_2^H is the concentration at saturation, and α_2 is the kinetic dissolution constant of the mineral.

Initial conditions ($t=0$) for the proposed experimental setup are:

$$N_1 = 0, \quad C_1 = C_1^0, \quad C_2 = C_2^0 \text{ for the adsorption stage,}$$

$$N_1 = N_0, \quad C_1 = 0, \quad C_2 = C_2^0 \text{ for the desorption stage.} \quad (18)$$

A general solution of system of Eqs. (15)–(17) for given initial conditions [Eq. (18)] can be written in the form of Eqs. (19) and (20) (see also Appendix A):

$$\bar{C}_1 = e^{-F(\bar{t})} \left[1 + \int_0^{\bar{t}} g(x) e^{F(x)} dx \right],$$

$$\bar{C}_1 = e^{-F(\bar{t})} \int_0^{\bar{t}} g(x) e^{F(x)} dx \quad (19)$$

for the adsorption ($\bar{C}_1 = C_1/C_1^0$) and desorption ($\bar{C}_1 = aC_1/N_0$) steps of the process, respectively;

$$F(\bar{t}) = \int_0^{\bar{t}} f(x) dx, \quad f(x) = \frac{1}{a} + \left(\bar{C}_2^0 \bar{C}_2 \right)^{\bar{z}}, \quad g(x) = \left(\bar{C}_2^0 \bar{C}_2 \right)^{\bar{z}},$$

$$\bar{C}_2 = \frac{C_2}{C_2^0}, \quad \bar{C}_2^0 = K_s^{z_2/z_1} C_2^0, \quad \bar{t} = \alpha_1 t, \quad \bar{\alpha} = \alpha_2/\alpha_1. \quad (20)$$

4.2.2. Fitting (typical) curves

Fig. 7a presents kinetic adsorption curves that were calculated for the exchange of univalent cations over a wide range of the dimensionless parameter $\bar{\alpha} = \alpha_2/\alpha_1$ for specified values $\bar{C}_2^H = C_2^H / C_2^0$, $\bar{C}_2^0 = K_s C_2^0$, $a = V\rho_b/m_s$ and $\bar{z}=1$.

In the general case ($10^{-4} < \bar{\alpha} < 1$), graphs are essentially nonmonotonic. The presence of a concentration minimum is explained by a competition of two reactions as discussed earlier in Section 3.2.2.

This kind of graph is qualitatively consistent with the results of the experiments conducted under elevated temperature and pressure. Two limiting cases may be associated with the asymptotic behavior of the function:

(1) if $\bar{\alpha} \ll 1$ then $\bar{C}_1 = a \frac{\bar{C}_2^0}{1 + a\bar{C}_2^0}$

(That is, dissolution proceeds slowly and practically does not influence the adsorption) and

(2) if $\bar{\alpha} \gg 1$ then $\bar{C}_1 = \frac{a\bar{C}_2^0\bar{C}_2^H}{1 + a\bar{C}_2^0\bar{C}_2^H}$

(That is, the rapid mineral dissolution leads to a quick saturation of the solution with the competing cation, which significantly suppresses the adsorption of the radionuclide).

In our example (Fig. 7a), the lower limiting value ($\bar{\alpha} \ll 1$) of \bar{C}_1 is 0.17 and the upper limiting values ($\bar{\alpha} \gg 1$) are 0.91 and 0.95 for $\bar{C}_2^H=50$ and $\bar{C}_2^H=100$, respectively.

Graphs of the step-by-step radionuclide desorption in the presence of a kinetically dissolving mineral are of some interest as well (Fig. 7b). According to the theoretical analysis, the calculated (effective) constant of the desorption distribution \bar{K}_d (dimension-

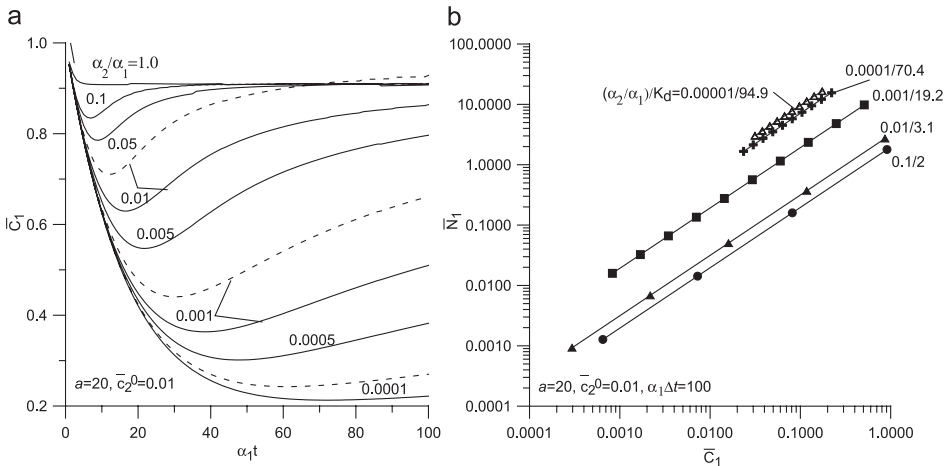


Fig. 7. Calculated curves reflecting: (a) a combined influence of radionuclide adsorption and mineral dissolution under unsteady-state condition (solid lines: $\bar{C}_2^H=50$, dotted lines: $\bar{C}_2^H=100$) and (b) calculated desorption isotherms (numbers on curves correspond to ratio $\bar{\alpha}$ to apparent distribution coefficient \bar{K}_d , $\alpha_1 \Delta t=100$). Calculations were carried out with $a=20$ and $\bar{C}_2^0=0.01$.

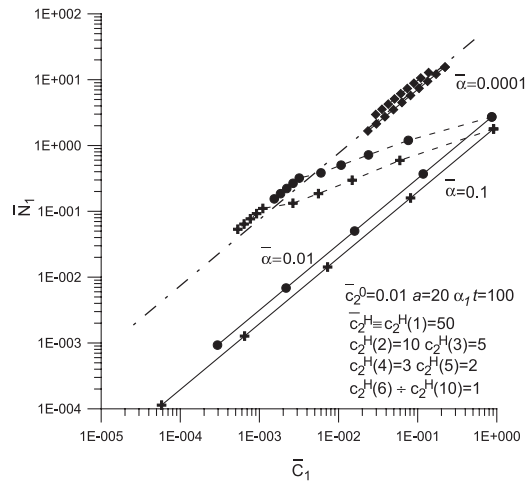


Fig. 8. Calculated desorption isotherms with $a=20$, $\bar{C}_2^0=0.01$, $\alpha_1 \Delta t=100$. Solid lines: $\bar{C}_2^H=50=\text{const}$, dotted lines: $\bar{C}_2^H=\bar{C}_2^H(i)$. Figures adjusted to the lines correspond to the value of $\bar{\alpha}$.

less parameter) ranges from $\bar{K}_d=(K_s C_2^0)^{-1}$ ($\bar{\alpha} \ll 1$) to $\bar{K}_d=(K_s C_2^0 \bar{C}_2^H)^{-1}$ ($\bar{\alpha} \gg 1$). The model isotherms are also controlled by the relationship of the kinetic constants $\bar{\alpha}=\alpha_2/\alpha_1$. Thus, in our example (Fig. 7b), the fitting constant of the desorption distribution \bar{K}_d ranges from 94.9, when $\bar{\alpha}=10^{-5}$ to 2.0, when $\alpha=0.1$. The values of \bar{K}_d depend on the duration of the adsorption and desorption step Δt as well. Lastly, a drop in the saturation concentration C_2^H from one desorption step to the next leads to a localization of the desorption points (N_i^d , C_i^d) on lines in coordinates $N-C$, which can be associated with nonlinear desorption isotherms (Fig. 8). This nonlinearity was noted in a number of experimental series. The observed hysteresis depends in this case on both variations in the values of C_2^H and on kinetics of the adsorption and dissolution processes. For example, if the desorption step of an experiment is characterized by a lower value of concentration C_2^H (compared with C_2^H of the adsorption stage), then the value of \bar{K}_d will be greater than what is predicted for the adsorption stage. This effect is encountered fairly often in practice. A decrease of the “effective” values of C_2^H from one experimental step to the next is explained by the gradual washout from rocks with a limited content of soluble salts (minerals).

5. Modeling results and discussion

An application of the model of heterogeneous sorption sites for the experiments with *Sr-90* is limited to the experimental series *Sr-GW-GW* because the hydrogeochemical environment remained nearly constant. In the remaining experiments, the kinetics of adsorption/desorption is overshadowed by dissolution processes of some constituents of the mineral phase that affects the adsorption kinetics and equilibrium. Experiments with *Cs-137* are less sensitive to the content of the major cations in the solution than those with

Sr-90, since Cs-137 prefers to adsorb on the rock in a no-exchange manner (Klechkovsky and Gulyakin, 1958; EPA, 1999).

5.1. Application of the kinetic model of dual-site adsorption

In the modeling discussed below, the value of the fraction (f) was assumed to be 0.75 because we considered that approximately 75% of the rock consists of minerals with the relatively weak mass-exchange (sorption) properties (quartz, feldspar, and carbonates; see Table 2). About 25 % would consist of the “active” mineral geosorbents (clay and micaceous minerals, Table 2). We also assumed that $n_1^d = n_1^s$ and $K_{F_i}^d = K_{F_i}^s$ and (with exception of series Sr-Na-GW).

5.1.1. Strontium-90

5.1.1.1. Experimental series Sr-GW-GW. The experimental points in Fig. 2a of the adsorption/desorption kinetics $C(t)$ fit sufficiently well with the predicted curves calculated using the parameters represented in Table 7. The use of the parameters obtained during the simulation of the step-by-step desorption are also in good agreement with the experimental and modeling points (Fig. 9a). The values of the predicted concentration C were, however, smaller than the experimental data for lower concentrations. This may be related to the nonlinearity of the process, which was not taken into account during the mathematical formalization of the problem.

An analysis of the values of the fitting constants (Table 7) yields the following: (1) the distribution coefficient for the clay fraction exceeds the values for the fraction ($K_{F_2}^s$) of quartz, plagioclase and carbonates ($K_{F_1}^s$), by a factor of about 50; (2) the kinetic desorption constants are noticeably smaller than the kinetic adsorption constants; and (3) $\alpha_2^d < \alpha_1^d$.

5.1.1.2. Experimental series Sr-Na-GW. The redistribution of the radionuclides between the reactive sorption sites at the desorption step results in the nonmonotonic behavior of the concentration function $C(t)$ (Fig. 2c). This can be modeled by increasing the value of the partial coefficient, $K_{F_2}^d$ which models the system as radionuclides released at the beginning of the experiments (i.e., the first hours) from the sites of type 1. These sites are characterized by the relatively low values of $K_{F_1}^s$ of and by the increased values of α_1^d . The radionuclides

Table 7
Fitting parameters of the adsorption–desorption experiments ($T=20\text{ }^\circ\text{C}$, $P=P_{\text{atm}}$)

n^s	n^d	$K_{F_1}^s$	$K_{F_2}^s$	$fK_{F_1}^s + (1-f)K_{F_2}^s$	α_1^s	α_2^s	α_1^d	α_2^d
Sr-90: adsorption/desorption in synthetic ground water (Sr-GW-GW)								
1.03	1.03	10	532	141	60	60	10	5
Sr-90: desorption by synthetic ground water (Sr-Na-GW)								
0.83	0.83	15	3000 ^a	761	100	100	15	3
Cs-137: adsorption/desorption in NaNO ₃ solution (Cs-Na-Na)								
0.89	0.89	20	300	90.0	70	50	15	7

^a $K_{F_2}^d$ value; units: $K_{F_i}^{s/d} \left[\left(\frac{\text{Bq}}{\text{cm}^3} \right)^{1-n^s} \right]$; $\alpha_i^{s/d} [d^{-1}]$; $K_{F_{1,2}}^s$: linear adsorption constants for sites of type 1 and 2, n : exponential constant adsorption/desorption; $\alpha_{1,2}^{s/d}$: kinetic adsorption/desorption constants for sites of type 1 and 2.

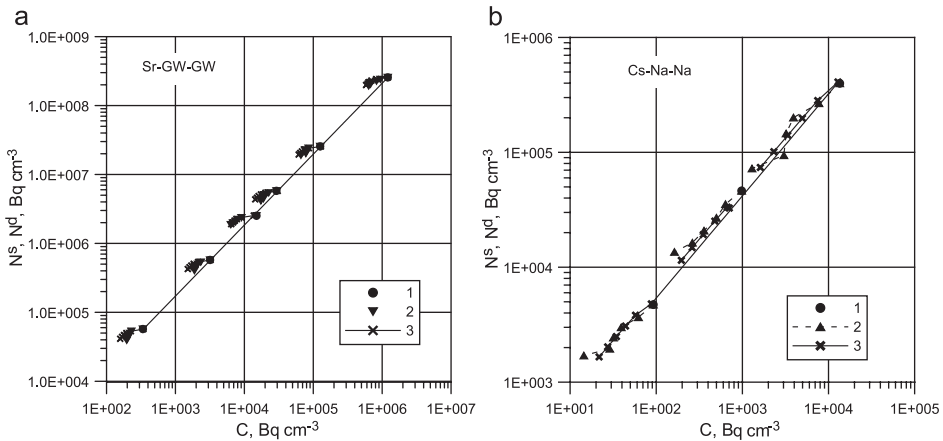


Fig. 9. Interpretation of the experimental adsorption–desorption isotherms: (a) series Sr-GW-GW [(1) adsorption, experimental data; (2) desorption, experimental data; (3) modeling results], (b) Cs-Na-Na [(1) adsorption, experimental data; (2) desorption, experimental data; (3) modeling results].

then start to be kinetically adsorbed by the sites of type 2 with the sharply increased values of the coefficient $K_{F2}^d (\gg K_{F1}^d)$ (Table 7). The overall effect of this model is the line shown in Fig. 2c.

5.1.2. Cesium-137

The adsorption–desorption stages of the experiment (series Cs-Na-Na) has been modeled using a dual-site adsorption model, which is in excellent agreement with

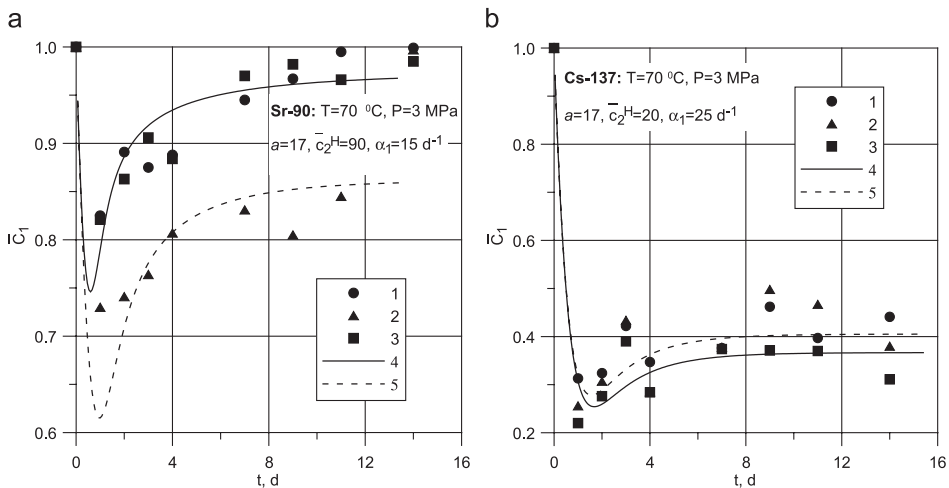


Fig. 10. Fitting curves for the adsorption kinetics of (a) Sr-90 [(1) $C_i=370,000 \text{ Bq cm}^{-3}$; (2) $C_i=37,000 \text{ Bq cm}^{-3}$; (3) $C_i=3700 \text{ Bq cm}^{-3}$; (4) $\bar{C}_2^0=0.02, \alpha_2/\alpha_1=0.01$; (5) $\bar{C}_2^0=0.004, \alpha_2/\alpha_1=0.02$] and (b) Cs-137 [(1) $C_i=37,000 \text{ Bq cm}^{-3}$; (2) $C_i=3700 \text{ Bq cm}^{-3}$; (3) $C_i=370 \text{ Bq cm}^{-3}$; (4) $\bar{C}_2^0=0.0017, \alpha_2/\alpha_1=0.02$; (5) $\bar{C}_2^0=0.002, \alpha_2/\alpha_1=0.02$].

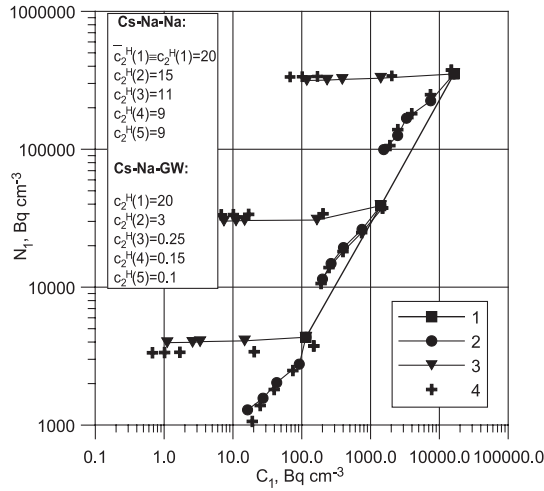


Fig. 11. Adsorption and desorption of Cs-137 (series Cs-Na-Na and Cs-Na-GW): experimental and modeling data. Crosses show results of calculations according to Eq. (19) with selected parameters: $\bar{C}_2^0=0.002$, $\alpha=0.02$, $\alpha_1=25d^{-1}$, $\Delta t=14d$, $a=17$ [(1) adsorption, (2) desorption: series Cs-Na-Na, (3) desorption: series Cs-Na-GW, (4) fitting points].

experimental data (dotted lines) (Figs. 2b and 9b). The values of fitting parameters for this model are given in Table 7; in particular the values of the kinetic constants (α_i^s) are close to the corresponding values obtained for Sr-90. Moreover, the same relationship seen for Sr-90 ($\alpha_i^d < \alpha_i^s$) was observed in these experiments.

5.2. Application of the one-site kinetic model of adsorption with concomitant dissolution of carbonate minerals

The experimental adsorption curves of Sr-90 at the elevated temperature and pressure (experimental series Sr-Na-70-3, Fig. 3a–c) exhibited a well-expressed extreme character. They are satisfactorily described with Eq. (19) using the fitting parameter (Fig. 10a). Experimental and modeling results agree when sufficiently low values of the dissolution kinetic constant are applied (e.g., $\bar{\alpha}=0.01–0.02$, $\alpha_2=0.15–0.30$ day⁻¹).

Experimental data on adsorption kinetics of Cs-137 (series Cs-Na-70-3, Fig. 3d–f) do not contradict the conceptual model as shown in Fig. 10b where values of the fitting parameters were obtained by substitution into Eq. (19). These parameters were also used for the calculation of isotherms presented in Fig. 11. In this procedure, the magnitude of the dimensionless concentration, $\bar{C}_2^H = \bar{C}_2^H(i)$ (where i is the number of the desorption step) was gradually decreased from one step to the next. The experimental and modeling values of C_1 and N_1 (for the specified values of a , \bar{C}_2^0 , $\bar{\alpha}$ and Δt) agreed with appropriate variations of the concentration, \bar{C}_2^H . The observed differences in the experimental and modeling results can be explained by a more complex nature of the relationship $N(C)$ in Eq. (9).

6. Conclusions

The following conclusions can be drawn from the results of batch experiments described in this paper:

(1) An analysis of the experimental data on the adsorption–desorption behavior of Sr-90 and Cs-137 indicates that the adsorption isotherms are of the Freundlich type. All experiments revealed hysteresis in radionuclide adsorption/desorption, which may result from alterations in the chemical composition of the solution. Temperature noticeably affects the radionuclide adsorption. In particular, the heating of the system leads to a decrease of the rock's adsorption capacity. Furthermore, the degree of nonlinearity correlates to increasing temperature. For radionuclides, which were previously adsorbed in the system of the background electrolyte, desorption becomes practically impossible under groundwater conditions: the process goes into the irreversible phase. The irreversible capture of ions by the crystalline phase occurs at elevated temperatures. It is also possible that an alteration of mineral phases occurs involving radionuclides.

(2) A kinetic dual-site model, which takes into account differences in adsorption/desorption constants, satisfactorily described experiments with Sr-90 in the groundwater system. This model can also be used for describing laboratory experiments with Cs-137 in the sodium nitrate solution at room temperature and atmospheric pressure. From this, the following is concluded: (a) kinetic desorption constants are lower than adsorption constants, so that complete chemical equilibrium may not be reached on the desorption steps (within a duration of several days to 2 weeks); (b) desorption from reactive sites of type 2 (clay and hydro-micaceous minerals) is characterized by the smaller kinetic constants than desorption from the reactive sites of type 1 (quartz and carbonate minerals), (c) the equilibrium linear coefficient of adsorption on the sites of type 2 increases after changing the composition of the solution of desorption sites in synthesized groundwater. This effect leads to a redistribution of radionuclides between the adsorption sites, and as a consequence, to the appearance of an extremum in the graph C versus t .

(3) An alternative interpretation of the hysteretic effects observed at elevated temperature and pressure is a model that accounts for the mutual interference of adsorption kinetics and dissolution of carbonate minerals. This coupled process results in a nonmonotonic behavior of the concentration curves at the adsorption stage. The model also explains a divergence of the adsorption and desorption branches on the isothermal graphs upon the sequential change of the solution's composition.

(4) Experimental results are important for the analysis of radionuclide migration in groundwater. Thus, the set up of the experiments can be associated with imitation ("static" modeling) of the groundwater system response to inflow of the acid brine into the aquifer. The behavior of the principal solution components in the experiments with unconditioned rock samples is similar to what is often observed at actual contaminated sites when the advancing front of an inflow solution displaces groundwater. In particular, such behavior was monitored at the Lake Karachai radioactive waste disposal site (the Southern Urals, Russia) (Rumynin et al., 1998) as well as at a number of sites in the Western Urals, Russia, where subsurface reservoirs of limestone and sandstone formations are contaminated by a chloride brine (Mironenko and Rumynin, 1999). Saturation of the solution with the

dissolution products of the soluble minerals of the rock matrix and ion-exchange reactions may be so high that adsorption of the radionuclides is essentially suppressed. In particular Sr-90 begins to behave similarly to a nonreactive chemical and migrates at the groundwater velocity. This conclusion is related to one of the most acute problems of environmental hydrogeology, namely to the problem of a “fast transport” of Sr-90 in subsurface environments. The “fast transport” of Sr-90 is a great practical interest for forecasting the propagation of the dissolved radioactive materials in groundwater.

Acknowledgements

This research was supported by the Swiss National Science Foundation (Grant No.7SUPJ062261) and the Russian Foundation for Basic Research (Grant No. 03-05-64231-à). The authors would like to thank E.V. Zakharova and E.P. Kaimin who were responsible for experimental part of this work. We also would like to thank the anonymous reviewers for their insightful comments and number of useful suggestions which helped us to reorganize the paper in more proper way.

Appendix A. Solution of the adsorption model with mineral dissolution kinetics

Eqs. (15) and (16) can be rewritten in a generalized dimensionless form:

$$\frac{d\bar{C}_1}{d\bar{t}} = \left[\left(\bar{C}_2^0 \bar{C}_2 \right)^{\bar{z}} - \left(\frac{1}{a} + \left(\bar{C}_2^0 \bar{C}_2 \right)^{\bar{z}} \right) \bar{C}_1 \right], \tag{A1}$$

where for the adsorptive process $\bar{C}_1 = \frac{C_1}{C_1^0}$ and for the desorption process $\bar{C}_1 = a \frac{C_1}{N_0}$;

$$\text{also } \bar{C}_2 = \bar{C}_2^H - \left(\bar{C}_2^H - 1 \right) e^{-\bar{\alpha}\bar{t}} \left(\bar{C}_2 = \frac{C_2}{C_2^0}, \bar{C}_2^H = \frac{C_2^H}{C_2^0} \right);$$

$$\bar{C}_2^0 = K_s^{z_2/z_1} C_2^0 \left(K_s^{z_2/z_1} = \frac{1}{K_{12}^{1/z_1} Q_v} \right); N_0 = a(C_1^0 - C_1^*); \bar{t} = \alpha_1 t, \bar{\alpha} = \alpha_2/\alpha_1.$$

Thus, the problem can be reduced to the solution of the following ordinary differential equation of the first order:

$$y' + f(\bar{t})y = g(\bar{t}), \tag{A2}$$

where $y \equiv y(\bar{t}) = \bar{C}_1, f(\bar{t}) = \frac{1}{a} + \left(\bar{C}_2^0 \bar{C}_2 \right)^{\bar{z}}, g(\bar{t}) = \left(\bar{C}_2^0 \bar{C}_2 \right)^{\bar{z}}$, with the transformed initial conditions (18):

$$\begin{matrix} \bar{N}_1 = 0 & \bar{C}_1 = 1 & \bar{C}_2 = 1, \\ \bar{N}_1 = 1 & \bar{C}_1 = 0 & \bar{C}_2 = 1 \end{matrix} \left(\bar{N}_1 = N_1/N_0 \right). \tag{A3}$$

Eq. (A2) can be solved with the help of a substitution $y=uv$ that leads to the transformation of Eq. (A2) as follows:

$$u\dot{v} + u[v' + vf(\bar{t})] = g(\bar{t}). \quad (\text{A4})$$

As one of the supplementary functions (u or v) can be taken arbitrary, we can consider v as some particular integral of Eq. (A5):

$$v' + vf(\bar{t}) = 0, \text{ or } \frac{dv}{v} = -f(\bar{t})d\bar{t}. \quad (\text{A5})$$

Then for the u function finding, we have Eq. (A6):

$$u\dot{v} = g(\bar{t}). \quad (\text{A6})$$

Having integrated Eq. (A5) we obtain:

$$v = v_0 e^{-F(\bar{t})}, v_0 = v(\bar{t} = 0), F(\bar{t}) = \int_0^{\bar{t}} f(x)dx. \quad (\text{A7})$$

Correspondingly, solution of Eq. (A6) is:

$$u = u_0 + \frac{1}{v_0} \int_0^{\bar{t}} g(x)e^{F(x)} dx, u_0 = u(\bar{t} = 0). \quad (\text{A8})$$

Finally,

$$y = uv = e^{-F(\bar{t})} \left[u_0 v_0 + \int_0^{\bar{t}} g(x)e^{F(x)} dx \right]. \quad (\text{A9})$$

As $u_0 v_0 = y_0$ is the initial concentration for $\bar{t} = 0$, then $u_0 v_0 = 1$ —for adsorption, and $u_0 v_0 = 0$ —for desorption.

Thus, the general solution of Eq. (A1) is as follows:

$$\begin{aligned} \bar{C}_1 &= e^{-F(\bar{t})} \left[1 + \int_0^{\bar{t}} g(x)e^{F(x)} dx \right], \\ \bar{C}_1 &= e^{-F(\bar{t})} \int_0^{\bar{t}} g(x)e^{F(x)} dx \end{aligned} \quad (\text{A10})$$

for the adsorption ($\bar{C}_1 = C_1/C_1^0$) and desorption ($\bar{C}_1 = aC_1/N_0$) steps of the process, respectively.

References

- Aksoyoglu, S., Bajo, C., Mantovani, M., 1990. Batch sorption experiments with iodine, bromine, strontium, sodium and cesium on Grimsel mylonite. Paul Scherrer Institute Report, PSI-Bericht Nr. 83. 50 pp.
- Charbeneau, R.J., 1982. Calculation of pollutant removal during restoration with adsorption and ion exchange. Water Resources Research 18 (4), 1117–1125.

- EPA, 1999. Methods for determining Kd values. in: Understanding variation in partition coefficient, Kd, values: Volume I. The Kd model, methods of measurement, and application of chemical reaction codes. EPA Report no. 402-R-99-004A. 310 pp.
- Golubev, V.S., 1981. The Dynamics of the Geochemical Processes. Nedra, Moscow. 208 pp. In Russian.
- Huang, W., Yu, H., Weber Jr., W.J., 1998. Hysteresis in the sorption and desorption of hydrophobic organic contaminants by soils and sediments: 1. A comparative analysis of experimental protocols. *Journal of Contaminant Hydrology* 31, 129–148.
- Jackson, R.E., Inch, K.J., 1983. Partitioning of strontium-90 among aqueous and mineral species in a contaminated aquifer. *Environmental Science and Technology* 17, 231–236.
- Jackson, R.E., Inch, K.J., 1989. The in-situ adsorption of Sr-90 in a sand aquifer at the Chalk River Nuclear Laboratories. *Environmental Science and Technology* 4, 27–50.
- Klechkovsky, V.M., Gulyakin, I.V., 1958. Behavior in soils and plants of the micro-quantities of strontium, cesium, ruthenium and zirconium. *Soil Science* (3), 1–15 (In Russian).
- Kokotov, Yu.A., Popov, R.F., 1962. The absorption of the long-life fission products by soils and by clay minerals: III. Selectivity of soils and clays regarding to ⁹⁰Sr under varied conditions. *Journal of Radiochemistry* 4 (3), 328–334 (In Russian).
- Kretschmar, R., Borkovec, M., Grolimund, D., Elimelech, M., 1999. Mobile subsurface colloids and their role in contaminant transport. *Advance in Agronomy* 66, 121–194.
- Lyon, K.E., Patterson, R.J., 1984. Evidence for non-equilibrium adsorption of ⁹⁰Sr from groundwater. *Water Pollution Research Journal of Canada* 19 (2), 23–34.
- Lisitzin, A.K., Sysoev, A.N., Ganina, N.I., Kartashev, L.F., Myskin, V.I., Nesterova, M.V., Schulik, H.P., 1999. Buffer geochemical properties of the geologic environment—Laboratory and Technological Studies of Mineral Raw. The Survey Information, vol. 4 (Geoinformmark. 60 pp., in Russian).
- Liszewski, M.J., Bunde, R.L., Hemming, C., Rosentreter, J., Welhan, J., 1998. The use of synthesized aqueous solutions for determining strontium sorption isotherms. *Journal of Contaminant Hydrology* 29, 93–108.
- Ma, L., Selim, H.M., 1994. Predicting atrazine adsorption–desorption in soils: a modified second-order kinetic model. *Water Resources Research* 30 (2), 447–456.
- Mironenko, V.A., Rumynin, V.G., 1999. Problems of environmental hydrogeology. Book 1: Applied Studies, vol. 3. MGGU Publ, Moscow (312 pp., in Russian).
- Ovsyanikova, S.V., Sokolik, G.A., Ejsmont, E.A., Kil'chitskaja, S.A., Kimlenko, I.M., Zhukovich, N.V., Rubinchik, S.J., 2000. Participation of soil solutions in migration of ¹³⁷Cs, ⁹⁰Sr, ^{239,240}Pu and ²⁴¹Am. *Geochemistry* (2), 222–234 (in Russian).
- Pickens, J.F., Jackson, R.E., Inch, K.J., Merritt, W.F., 1981. Measurement of distribution coefficient using a radial injection dual-tracer test. *Water Resources Research* 17 (3), 529–544.
- Rumynin V.G., Mironenko V.A., Sindalovsky L.N., Boronina A.V., Konosavsky P.K., Pozdniakov S.P., 1998. Evaluation of conceptual, mathematical and physical-and-chemical models for describing subsurface radionuclide transport at the Lake Karachai waste disposal site. Lawrence Berkeley National Laboratory Report, LBNL-41974. 70 pp.
- Rumynin, V.G., Konosavsky, P.K., Hoehn, E., 2002. Batch laboratory, analytical and modeling study of subsurface transport of irreversibly adsorbing Sr-90. Proceedings of the 4th International Conference on Calibration and Reliability in Groundwater Modelling (ModelCare'02). Czech Republic, Prague, pp. 429–432. June 17–20.
- Rybalchenko, A.I., 1998. Deep-well injection of liquid radioactive waste in Russia: present situation. In: Stenhous, M.J., Kirko, V.I. (Eds.), *Defence Nuclear Waste Disposal in Russia: International Perspective*. NATO ASI Series, Disarmament Technologies, vol. 18. Kluwer Academic Publishers, pp. 199–217.
- Rybalchenko, A.I., Pimenov, M.K., Kostin, P.P., 1994. A deep injection of liquid radioactive waste into geological formation. Atomic Energy Publ, Moscow (256 pp., In Russian).
- Rybalchenko, A.I., Pimenov, M.K., Kurochkin, V.M., 1996. Scientific and practical results of the deep-injection disposal of liquid radioactive wastes in Russia. In: Apps, J.A., Tsang, C.-F. (Eds.), *Deep Injection Disposal of Hazardous and Industrial Waste. Scientific and Engineering Aspects*. Academic Press, pp. 657–662.
- Selim, H.M., Amacher, M.C., 1988. A second-order kinetic approach for model solute retention and transport in soils. *Water Resources Research* 24, 2061–2075.
- Strech, Th., Poletika, N.N., Jury, W.A., Farmer, W.J., 1995. Description of simazine transport with rate-limited two-stage, linear and nonlinear sorption. *Water Resources Research* 31 (4), 811–822.

- Tiknor, K.V., Cho, Y.-H., 1990. Interaction of iodide and iodate with granitic fracture-filling minerals. *Journal of Radioanalytical and Nuclear Chemistry Articles* 140 (1), 75–90.
- Vandergraaf, T.T., Abry, D.R.M., 1982. Radionuclide sorption in drill core material from the Canadian Shield. *Nuclear Technology* 57, 399–412.
- Van de Weerd, H., Leijnse, A., 1997. Assessment of the effect of kinetics on colloid facilitated radionuclide transport in porous media. *Journal of Contaminant Hydrology* 26 (1–4), 245–256.
- Van Genuchten, M.T., Wagenet, R.J., 1989. Two-site/two-region models for pesticide transport and degradation: theoretical development and analytical solutions. *Soil Science Society of America Journal* 53, 1303–1310.
- Vilks, P., Degueldre, C., 1991. Sorption behavior of ^{85}Sr , ^{131}I and ^{137}Cs on colloids and suspended particles from the Grimsel Test Site, Switzerland. *Applied Geochemistry* 6, 553–563.
- Vilks, P., Cramer, J.J., Bachinski, D.B., Doern, D.C., Miller, H.G., 1993. Studies of colloids and suspended particles, Cigar Lake uranium deposit, Saskatchewan, Canada. *Applied Geochemistry* 8, 605–616.
- Weber Jr., W.J., Huang, W., Yu, H., 1998. Hysteresis in the sorption and desorption of hydrophobic organic contaminants by soils and sediments: 2. Effects of soil organic matter heterogeneity. *Journal of Contaminant Hydrology* 31, 149–165.
- Wels, C., Smith, L., Vandergraaf, T.T., 1996. Influence of specific surface area on transport of sorbing solutes in fractures. *Water Resources Research* 7, 1943–1954.
- Yegorov, Yu.V., Pushkarev, V.V., Tkachenko, E.V., 1961. The co-precipitation of the microquantities of ^{90}Sr with the active manganese dioxide in the presence of macro-quantity of barium and potassium. *Journal of Radiochemistry* 1, 87–89 (in Russian).
- Zakharova, E.V., Kaimin, E.P., Mikerin, E.I., Kudryavtsev, E.G., Rybalchenko, A.I., 1996. Behavior of radionuclides in geologic formation used for underground disposal of liquid nuclear wastes. In: Apps, J.A., Tsang, C.-F. (Eds.), *Deep Injection Disposal of Hazardous and Industrial Waste*. Scientific and Engineering Aspects. Academic Press, pp. 663–668.